

launch vehicles (Vongpaseuth *et al.* (1995)). These engines make use of a combination of low and high-density fuels to meet the varying thrust requirements. Altitude compensation nozzle is an inevitable part of long-duration missions as conventional non-adapted bell nozzles lead to a loss in propulsive efficiency (Hagemann *et al.* (2004)). Dual throat nozzle (DTN) is a suitable passive altitude adaptive nozzle (Ewen and O'Brien (1986)) consisting of a primary nozzle and a secondary nozzle which are independently operated from different thrust chambers as shown in Fig. 1. The primary (inner) nozzle expands low-density fuel oxidizer mixture, whereas the secondary (outer) nozzle expands the high-density fuel oxidizer mixture (Lundgreen *et al.* (1978)). Altitude compensation is achieved by controlling the chamber pressure of the secondary nozzle.

Dual throat nozzles used in tri-propellant engines consist of a supersonic reacting flow field of species emanating from independent thrust chambers (Nguyen *et al.* (1988)). The existence of a supersonic free shear layer separating two working fluid streams with active reacting species and shock train makes the flow field complex to analyze. The present numerical study envisages characterizing the turbulent reacting flow field resulting in a DTN during the simultaneous operation of the thrust chambers powered by RP_1 - O_2 and H_2 - O_2 combustion. Modeling of chemical reactions in the flow field is carried out using accurate multi-step reaction mechanisms for the oxidation of each fuel. The turbulent reacting shear layer resulting due to the supersonic combustion of two different types of fuels in the presence of a shock system is the key aspect of the present problem.

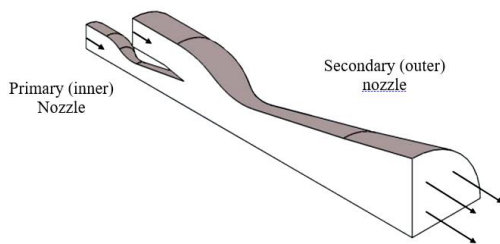


Fig. 1. Schematic of a dual throat nozzle (DTN).

2. LITERATURE REVIEW

The advent of high-pressure bipropellant engines and tri-propellant engines for single-stage-to-orbit and heavy-lift launch vehicles mooted the dual throat concept (Martin, 1996). Meagher (1981) carried out extensive studies and parametric analyses for both dual throat and dual expander nozzles. Aerojet Liquid Rocket Company carried out a performance analysis of a NASA-MSFC designed dual-throat thruster (O'Brien (1982)). A series of tests with various levels of both thrust chambers have been performed to ascertain the required parallel flow performance. TPEs are commonly used in a mixed-mode propulsion

scheme for the SSTO mission. Goracke *et al.* (1995) compared various Tri-propellant engine alternatives and suggested an optimum mixture ratio of propellants for various operating conditions.

Significant improvement in the performance of a conventional nozzle is possible with altitude adaptation by minimizing the losses incurred during the over/under expansion process. Hagemann *et al.* (1998) compared various types of altitude adapting nozzles to assess their performance enhancement over conventional nozzle design by altitude compensation. Two-position nozzle, dual bell nozzle, and dual expander nozzle are altitude adapting concepts similar to the dual throat concept dealt in the present study. The dual-throat fluidic thrust-vectoring nozzle concept for thrust vectoring applications (Deere, 2003). A conventional shock vector control method makes use of a secondary fluid stream to deflect the primary supersonic flow with the oblique shock waves. Adapting the dual throat nozzle geometry for the necessary thrust vectoring can also be made possible (Wang *et al.* 2017). Though DTN is used for thrust vectoring applications, flow features resulting in those scenarios are entirely different that found in DTN used for TPE applications.

Compressible turbulent reacting flow simulations (Deepu *et al.* (2017)) can depict the physio-chemical evolution in complex supersonic flow fields involving shock trains. Realistic numerical simulation of the tri-propellant engine is not common in literature. Turbulent reacting flow simulations using Navier-Stokes solver with apt multi-step chemical kinetics and thermal property model are essential to predict the evolution of complex features and viscous flow effects in a DTN flow field.

Numerical simulation of propulsion systems is helpful in performance prediction. Recently Shyji *et al.* (2017) simulated flow and reaction processes inside a high area ratio nozzle with secondary injection. The basic numerical framework dealt in the present study is similar to the well-validated and established procedure given in this work. The combustion modeling presented in the current work is quite involved due to the presence of two different types of fuels and many species resulting due to the reaction.

3. SOLUTION METHODOLOGY

The Navier-Stokes equations have been solved along with Menter's (1994) SST $k-\omega$ turbulence model and finite rate chemistry models for the simulation of supersonic flow and combustion of propellants in individual thrust chambers and dual throat nozzle.

Continuity equation

$$\frac{\partial \rho}{\partial t} + \frac{\partial}{\partial x_i} (\rho u_i) = 0 \quad (1)$$

Momentum equation

$$\frac{\partial}{\partial t}(\rho u_i) + \frac{\partial}{\partial x_i}(\rho u_i u_j) = -\frac{\partial p}{\partial x_i} + \frac{\partial \tau_{ij}}{\partial x_i} \quad (2)$$

Energy equation

$$\frac{\partial}{\partial t}(\rho e) + \frac{\partial}{\partial x_i}(\rho u_i e) = \frac{\partial p}{\partial t} + \frac{\partial}{\partial x_i} \left[\mu \left(\frac{1}{Sc_k} - \frac{1}{Pr} \right) \sum_{k=1}^N e_k \frac{\partial Y_k}{\partial x_i} + \frac{\mu}{Pr} \frac{\partial e}{\partial x_i} \right] \quad (3)$$

Species transport equation

$$\frac{\partial}{\partial t}(\rho Y_k) + \frac{\partial}{\partial x_i}(\rho u_i Y_k) = \frac{\partial}{\partial x_i} \left(\rho D_c \frac{\partial Y_k}{\partial x_i} \right) + S_{Y_k} \quad (4)$$

The turbulent kinetic energy equation

$$\frac{\partial(\rho \kappa)}{\partial t} + \frac{\partial(\rho u_i \kappa)}{\partial x_i} = \tilde{P}_\kappa - \beta^* \rho \omega \kappa + \frac{\partial}{\partial x_i} \left[(\mu + \sigma_\kappa \mu_t) \frac{\partial \kappa}{\partial x_i} \right] \quad (5)$$

The specific dissipation rate equation

$$\begin{aligned} \frac{\partial(\rho \omega)}{\partial t} + \frac{\partial(\rho u_i \omega)}{\partial x_i} = & \gamma \rho S^2 - \beta \rho \omega^2 + \frac{\partial}{\partial x_i} \left[(\mu + \sigma_\omega \mu_t) \frac{\partial \omega}{\partial x_i} \right] \\ & + 2(1 - F_1) \frac{\rho \sigma_{\omega 2}}{\omega} \frac{\partial \kappa}{\partial x_i} \frac{\partial \omega}{\partial x_i} \end{aligned} \quad (6)$$

F_1 is the blending function and other the closure coefficients are $\beta^* = 0.09$,

$$\left. \begin{array}{l} \beta = 0.075 \\ \sigma_{\omega 1} = 0.65 \\ \sigma_{\kappa 1} = 0.85 \end{array} \right\} \text{for } \kappa - \omega \text{ and } \left. \begin{array}{l} \beta = 0.0828 \\ \sigma_{\omega 2} = 0.856 \\ \sigma_{\kappa 2} = 1 \end{array} \right\} \text{for } \kappa - \varepsilon$$

Chemical species modeled rate of due to reactions is estimated using the law of mass action as

$$\sum_{i=1}^{N_s} \gamma'_{ji} C_i \xrightleftharpoons[k_{bj}]{k_{fi}} \sum_{i=1}^{N_s} \gamma''_{ji} C_i \quad (7)$$

Here k_f and k_b are the forward and backward reaction rates which are expressed in Arrhenius form.

$$S_{Y_i} = W_i \left[\left(\gamma'_{ji} - \gamma''_{ji} \right) \left(k_{fi} \prod_{i=1}^N C_i^{\gamma'_{ji}} - k_{bi} \prod_{i=1}^N C_i^{\gamma''_{ji}} \right) \right] \quad (8)$$

where $i = 1, 2, 3, \dots, N_s$ represents species and $j = 1, 2, 3, \dots, N_r$ represents reactions.

The total energy of the flow field is

$$E = \sum_{i=1}^{N_s} Y_i e_i - \frac{p}{\rho} + \frac{1}{2} (u_i^2) \quad (9)$$

The pressure in the flow field is calculated as

$$p = \rho R_u \sum_{i=1}^{N_s} \frac{Y_i}{W_i} T \quad (10)$$

here the R_u is the universal gas constant and temperature T is calculated from total energy.

The present dual throat problem involves the combustion of two different propellants in individual thrust chambers and while flowing dual throat nozzle. An extensive 8 species 18 step model finite chemistry mechanism proposed by [Drummond *et al.* \(1987\)](#) is used to model H₂-O₂ reaction. Kerosene (RP1) combustion chemistry is modeled using the reaction mechanism suggested by [Wang \(2001\)](#), which includes a naphthalene global step (C₁₂H₂₄+6O₂ → 12CO+12H₂) and a 3 step wet CO mechanism. Details of H₂-O₂ and wet CO mechanisms are summarized in Table 1.

The RANS equations for a compressible turbulent reacting flow with HLLC scheme make solved using the METACOMP CFD++ code. This features a Total Variation Diminishing (TVD) discretization based on a multi-dimensional interpolation framework. The HLLC (Harten, Lax, van Leer, with Contact wave) Riemann solver computes the upwind fluxes ([Palaniswamy *et al.* 2001](#)). This type of Riemann solvers is more robust for high-speed flows than the linear Roe family schemes ([Toro *et al.* 1994](#)). The HLLC scheme introduced by [Toro \(2009\)](#) is a modification to the existing HLL scheme, where the missing contact and shear waves in the Euler equations are restored. There is no contact discontinuity in the HLLC scheme. The complex shock system and sharp gradients existing in the present supersonic reacting flow field have been successfully captured using this scheme. Implicit time integration has been chosen and the convergence is ensured by allowing the residuals to fall below 1×10⁻⁶ in every time-step. About 120 iterations are required to meet convergence of all conservation variables. The double precision has been used for all the computations.

4. SOLVER VALIDATION

The present numerical solution procedure has been validated using a benchmark experimental data of the supersonic coaxial combustion test case. [Cheng *et al.* \(1991\)](#) experimented to measure the temperature and individual reacting species concentration using UV Raman scattering techniques. A comprehensive set of data is available and this enables a good platform for ensuring the predictability of major variables involved in the problem. This has been widely used for the validation of supersonic reacting flow solvers ([Deepu *et al.* 2007](#)). Hydrogen and air streams are in supersonic, conditions and undergo non-premixed combustion in the shear layer formed between the coaxial jets. The computational domain for the simulation of the Cheng's burner is given in Fig. 2. The entire computational domain has been initialized with ambient conditions. Flow conditions imposed for the coaxial streams are summarized in Table 2. Domain was discretized to 300 × 90 control volumes and progressively refined to 600 × 120 and 900 × 180 control volumes in the coaxial jet regime. The variation in species profile data was within 1.0% between the second and third level of refinement. Hence, the grid corresponds to the second level of refinement (600 × 120) has been

Table 1 Finite chemistry models for H₂-O₂ reaction (18 steps model) and wet CO mechanism

Reaction	Forward Reaction Rates		
	A	N	E
$H_2 + O_2 \leftrightarrow 2 OH$	0.7×10^{11}	0.0	0.20159×10^9
$O_2 + H \leftrightarrow OH + O$	0.142×10^{12}	0.0	0.6866×10^8
$H_2 + OH \leftrightarrow H_2O + H$	0.316×10^5	1.8	0.12686×10^8
$H_2 + O \leftrightarrow OH + H$	0.207×10^{12}	0.0	0.57568×10^8
$2 OH + O \leftrightarrow H_2O + O$	0.55×10^{11}	0.0	0.29307×10^8
$OH + H + M \leftrightarrow H_2O + M$	0.221×10^{22}	-2.0	0
$H + H + M \leftrightarrow H_2 + M$	0.653×10^{12}	-1.0	0
$O_2 + H + M \leftrightarrow HO_2 + M$	0.32×10^{13}	-1.0	0
$OH + HO_2 \leftrightarrow O_2 + H_2O$	0.5×10^{11}	0.0	0.4186×10^7
$H + HO_2 \leftrightarrow H_2 + O_2$	0.253×10^{11}	0.0	0.29307×10^7
$H + HO_2 \leftrightarrow 2 OH$	0.199×10^{12}	0.0	0.7536×10^7
$O + HO_2 \leftrightarrow O_2 + OH$	0.5×10^{11}	0.0	0.4186×10^7
$2 HO_2 \leftrightarrow O_2 + H_2O_2$	0.199×10^{10}	0.0	0
$H_2 + HO_2 \leftrightarrow H + H_2O_2$	0.301×10^9	0.0	0.7829×10^8
$OH + H_2O_2 \leftrightarrow H_2O + HO_2$	0.102×10^{11}	0.0	0.7954×10^7
$H + H_2O_2 \leftrightarrow H_2O + OH$	0.5×10^{12}	0.0	0.4186×10^8
$O + H_2O_2 \leftrightarrow OH + HO_2$	0.199×10^{11}	0.0	0.247×10^8
$H_2O_2 + M \leftrightarrow 2 OH + M$	0.121×10^{15}	0.0	0.19049×10^9
$CO + OH \leftrightarrow H + CO_2$	4×10^{12}	0.0	4.030×10^3
$CO + O_2 \leftrightarrow CO_2 + O$	3×10^{12}		2.5×10^4
$CO + O + M \leftrightarrow CO_2 + M$	6×10^{13}		0

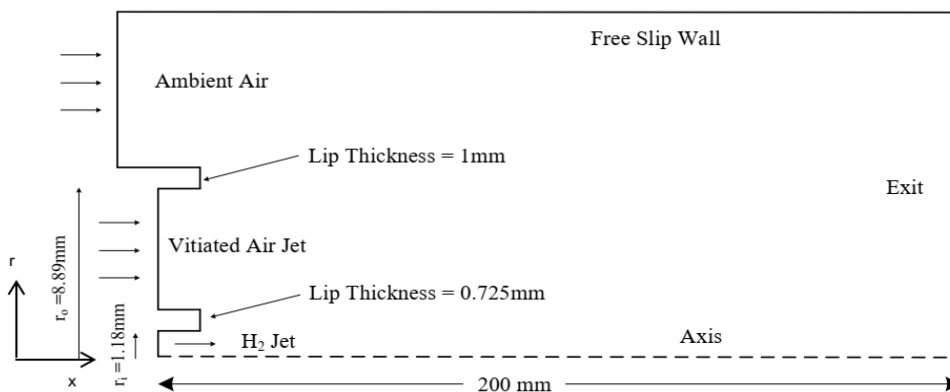
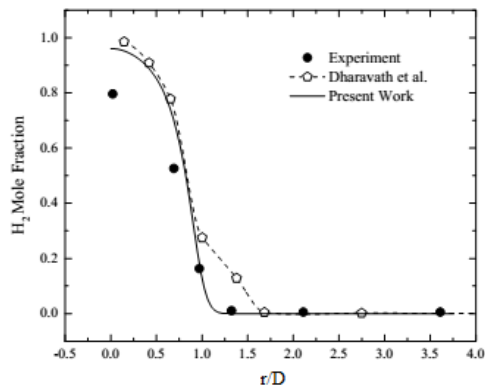


Fig. 2. Computational domain for validation test.

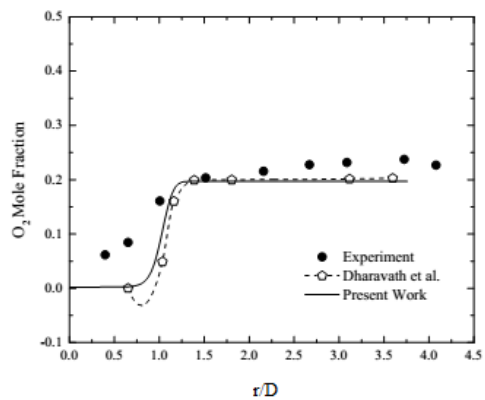
used for further studies and comparison. Minimum cell size is in the order of 10^{-5} in both shear layers.

The axial distance is normalized with diameter of the H₂ jet ($D=2.36$ mm). A comparison of the

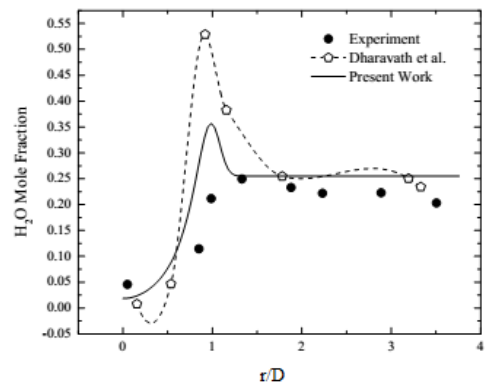
predicted species profiles in the reacting coaxial shear layer with the aforementioned experiment and another recent 3D-RANS computational study (Dharavath *et al.* (2017)) for a location $x/D = 10.8$ is shown in Fig. 3.



(a) Hydrogen mass fraction



(b) Oxygen mass fraction



(c) Water mass fraction

Fig. 3. Comparison of computed species profile in the shear layer with experiment [Cheng *et al.* (1991)] and another RANS simulation [Dharavath *et al.* (2017)] for a location $x/D = 10.8$.

An overall agreement between present computational results with that of the reported experimental and computational data can be observed. A maximum deviation of 12-15% for the H_2 and O_2 mole fractions is observed in the core region of the jet where mixing effects are minimum. Good agreement has been obtained in the shear

layer region (within 1%). The major reason for the uncertainties reported in the experimental data (Cheng *et al.* 1991) for both concentration and temperature measurements is photon statistics shot noise. The experimental relative standard deviation for concentrations is 6.3% in a stoichiometric flame at 2300K and 11.7% for temperature measurement. Minor disagreements of the present numerical results have been attributed to the three-dimensionality in actual experimental conditions. Hence the present results are compared with a 3D RANS simulation, which yielded a good comparison.

Table 2 Flow conditions at the inlet of the computational domain

Parameter	H_2 Jet	Vitiated air jet	Ambient
Mach Number	1	2	0
Pressure (kPa)	112	107	101
Temperature (K)	545	1250	300
H_2 mass Fraction	1.0	0	0
O_2 mass Fraction	0	0.24	0.23
H_2O mass Fraction	0	0.175	0.01

Contour plots of the salient variables in the problem such as Mach number, temperature, and mole fraction of water are given in Fig. 4. The complex nature of the present turbulent compressible reacting shear layer is evident from the Mach number contour. Coaxial jets and resulting shear layer progress through a series of expansion and compression waves, which constantly perturb the stream. The temperature contour indicates that the ignition happens after the mixing of the coaxial streams of fuel and the oxidizer. This aspect is also evident in water mole fraction contour. Mixing is controlled by the recirculation anchored to the lip region at the inlet. A significant improvement in mixing attributed by the continuous shock-expansion wave interaction promotes further reaction effects and hence leads to more heat release in downstream locations. The results of the validation studies indicate that the present solver is robust in the simulation of high-speed compressible reacting flows.

5. REACTING FLOW SIMULATIONS FOR DUAL THROAT THRUSTERS

Extensive computational exercises have been performed to portray the complex physics resulting from the supersonic mixing and reaction in the shear layers emanating due to the interaction of combustion products emanating from thrust chambers in a dual throat rocket thruster. As a typical operating condition, the dual throat thruster operating in parallel mode is considered. Hydrogen and kerosene (RP1) are the fuels burnt in the primary and secondary thrust chambers respectively, with oxygen as the common propellant. The computational domain used for the present study is given in Fig. 5. The boundary

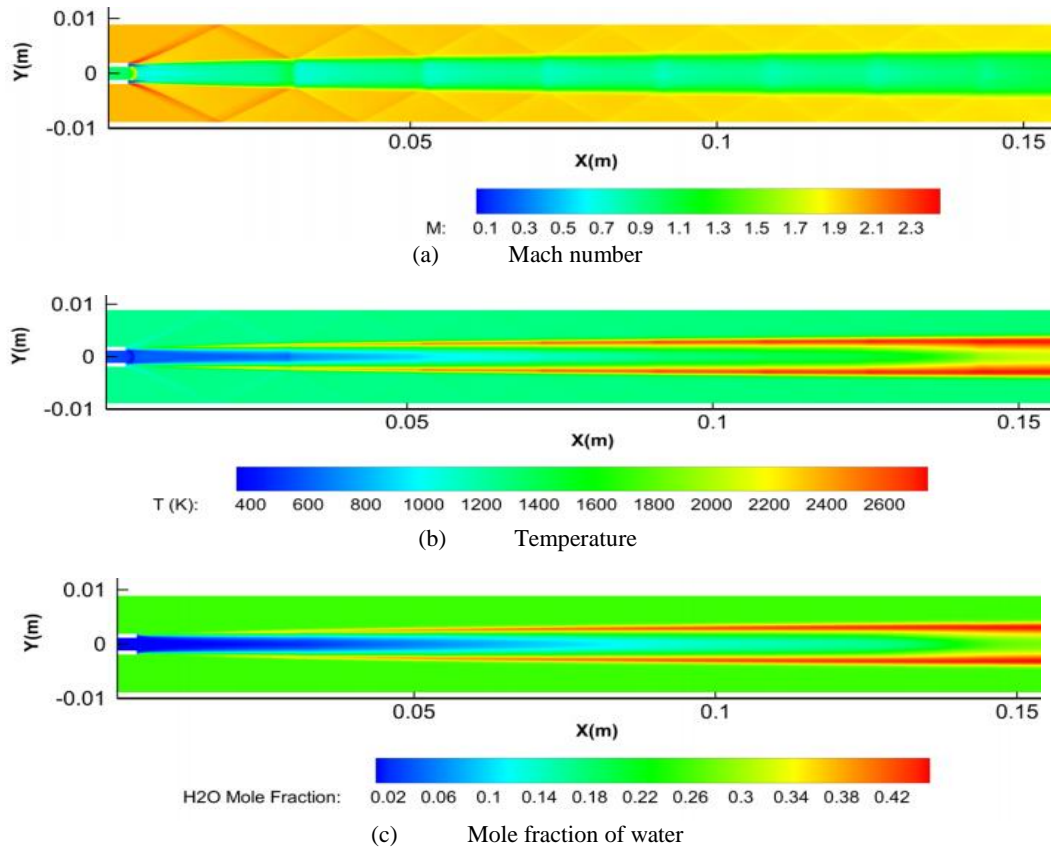


Fig. 4. Contours of variables in the flow field.

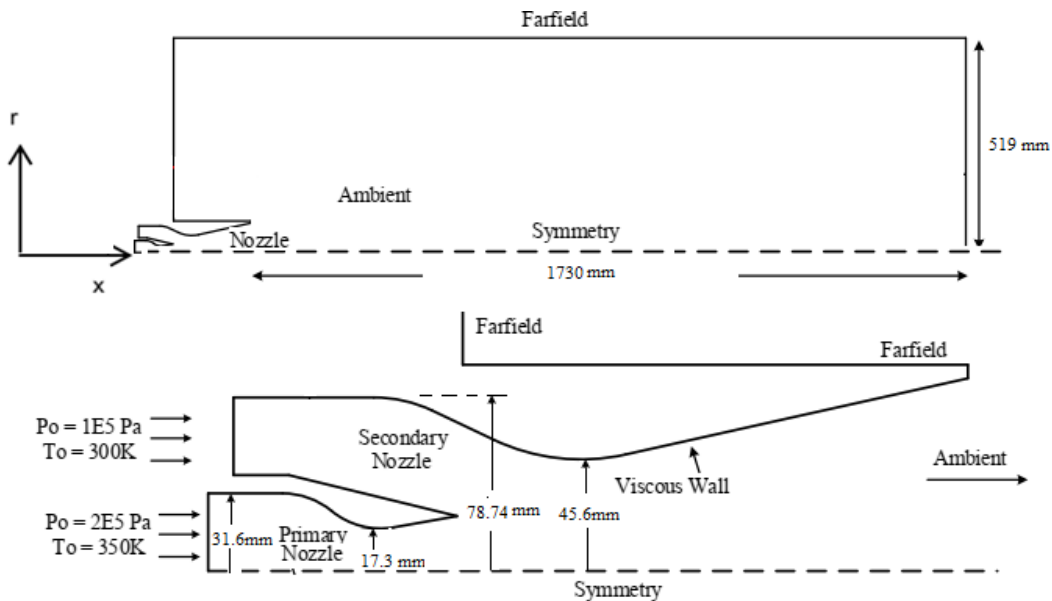


Fig. 5 Computational domain for the DTN simulation.

conditions implemented at the inlet of both the nozzles are summarized in Table 3.

Three different grid levels were used for the grid independency study, by providing $375 \times 50,700 \times 100$ and 1075×200 grids within the DTN area. Normalized wall pressure for the primary and secondary nozzles are compared for the various

level of refinement (Fig. 6). Results are in good agreement for the second and third levels of refinement. A comparison of mass flow rate and thrust of the nozzle for different grid levels is given in Table 4. The grid corresponding to 700×100 has been selected for further analysis.

Mach contours obtained from the simulation of the

dual throat thruster is shown in Fig. 7. The characteristics of the transformation of the low-velocity shear layer formed across coaxial expanding supersonic streams are evident in this figure. Shock formed at the exit of the inner nozzle brings down the momentum of the stream which enables the outer stream to deflect more in the core. A smooth transition of the annulus flow from subsonic to supersonic conditions is ensured at these conditions. There exists a low-velocity region near the exit of the inner nozzle which anchors the shear layer. Streamlines are superimposed with X velocity contours and shown in Fig. 8. Streamline deflections across oblique shocks can be visualized in this figure. The shear layer existing within expanding supersonic streams of differing speed levels has a unique variation across various cross-sections downstream of the inner nozzle.

Table 3 Flow conditions at the inlet of the computational domain of dual throat thruster

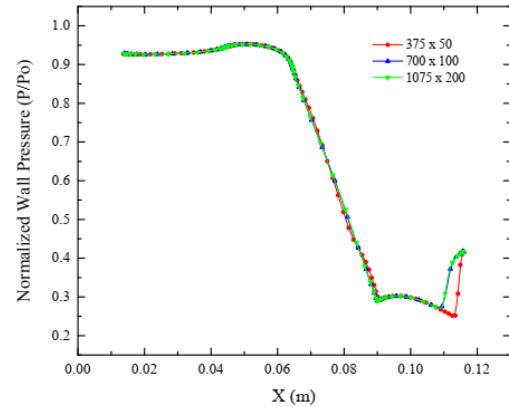
Parameter	Inner chamber	Outer chamber
Stagnation Pressure (MPa)	13.79	6.89
Stagnation Temperature (K)	3680	3701
H ₂ mass Fraction	0.0215316	0.0053683
H mass Fraction	0.0019406	0.0011437
O ₂ mass Fraction	0.0246415	0.0444141
O mass Fraction	0.0071798	0.0114485
H ₂ O mass Fraction	0.8657248	0.2441791
OH mass Fraction	0.0789817	0.0533617
CO mass Fraction	0	0.3308595
CO ₂ mass Fraction	0	0.3092251

Table 4 Details of grid independence study

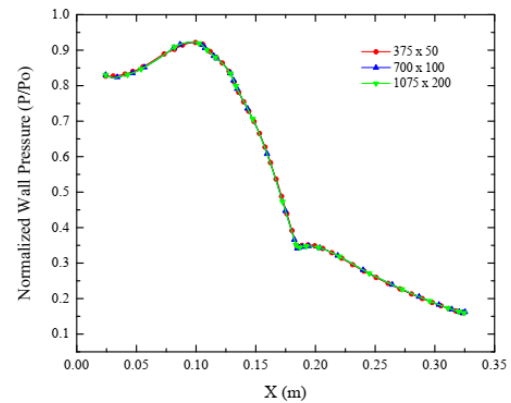
Grid Size in DTN area	mass flow rate (kg/s)	Thrust (N)
375×50	13.25	8501
700×100	13.29	8524
1075×200	13.29	8524

Parallel operation of both thrust chambers in a dual throat thruster for a typical low altitude condition gives interesting shock interaction features as shown in Fig. 9. Numerical Schlieren plot provides the second-order gradients of density in the flow field, enables to visualize sharper gradients formed due to shocks. The presence of normal shocks and flow separation at the diverging section of the primary nozzle is formed due to the backpressure imposed by the secondary flow during parallel flow operation. This particular operating condition selected for the present study has resulted in a Mach reflection pattern of shock interaction in the dual throat nozzle flow field comprising of an incident

shock, reflected shock, and the Mach stem is found to confine within the high-speed shear layer. This flow structure is subjected to a gradual variation when there is a change in ambient conditions during the ascend of the space vehicle.



(a) Normalized wall pressure for the primary nozzle



(b) Normalized wall pressure for the secondary nozzle

Fig. 6. Results of the grid independence study.

The profiles of the x-velocity component in the high-speed shear layer from 0.122m to 0.154 m downstream of the throat of the inner nozzle are shown in Fig. 10. The shear layer thickens as it flows downstream. Shock interaction and the reaction of active species exhibit an interesting static temperature pattern (Fig. 11) in dual throat thruster. A sudden rise in static temperature rise is observed in the downstream of the inner nozzle where shock interacts. Heat release due to the reaction effects in the shear layer contributes further to the heat generation. Both streams eventually cool as flow expands further in the outer diffuser.

A sudden change in static temperature marked by the presence of the shock system brings substantial changes in the concentration of free radicals and combustion products. Variation of water mass fraction across normal shock at the exit of the inner nozzle is shown in Fig. 12. A similar discontinuous pattern of all active species and products is observed across the shock system at the exit of the inner nozzle (Fig.13).

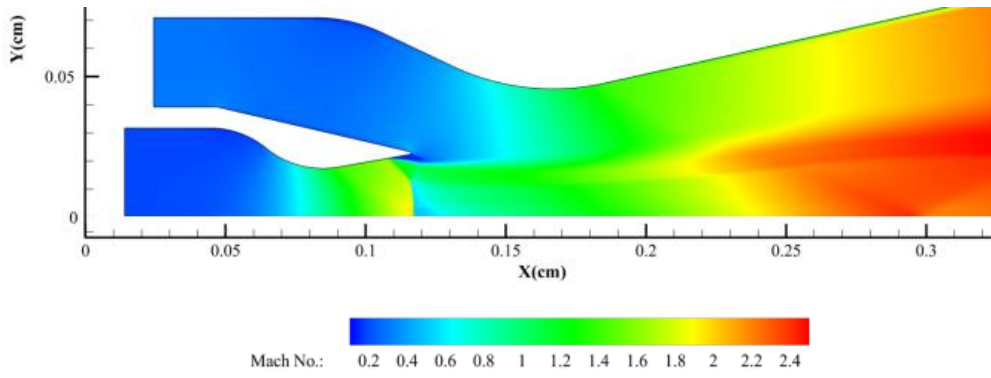


Fig. 7. Mach contours in the DTN flow field.

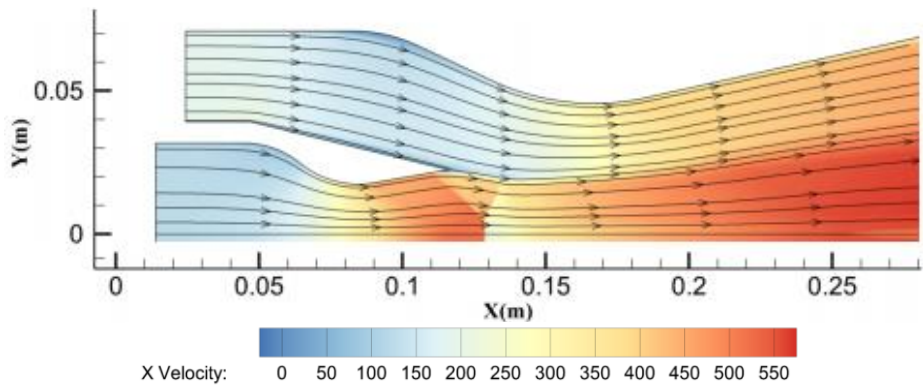


Fig. 8. A contour plot of x-velocity component and streamlines.

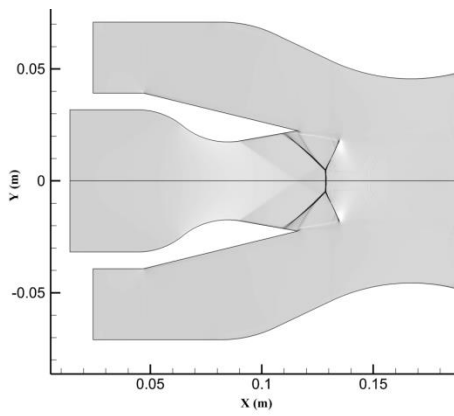


Fig. 9. Numerical Schlieren of the DTN flow field.

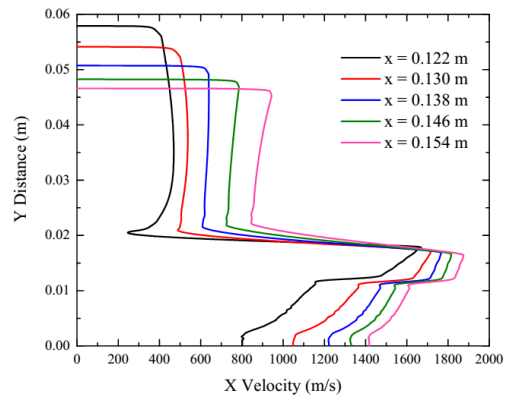


Fig. 10. X velocity component profiles in the high-speed shear layer.

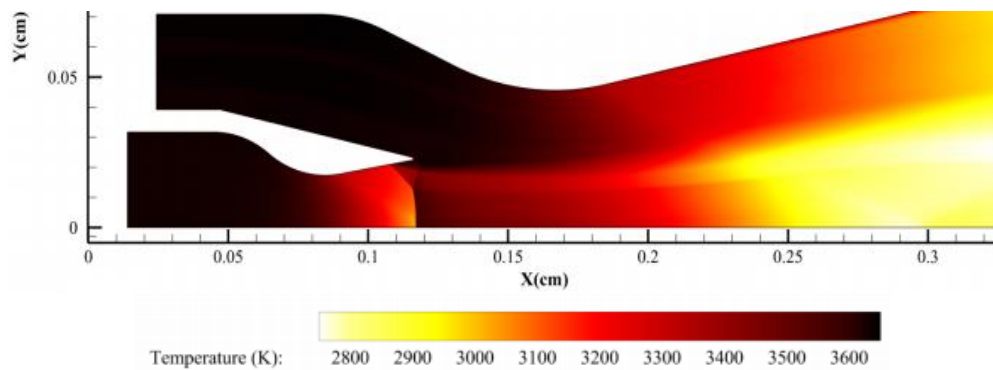


Fig. 11. Temperature contours in the DTN flow field.

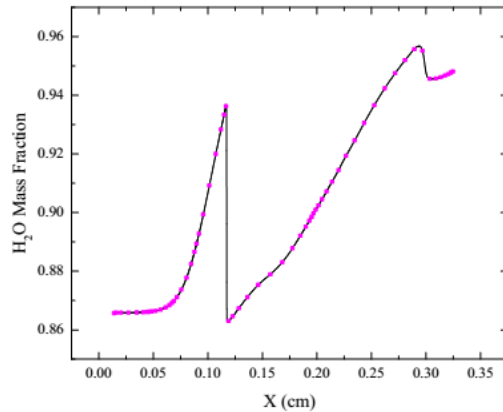


Fig. 12. Variation of water mass fraction across normal shock in DTN.

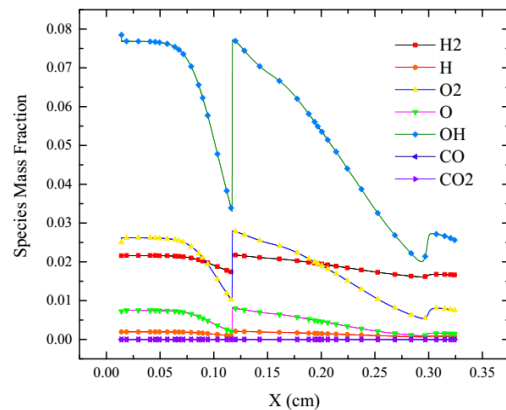


Fig. 13. Variation of species mass fraction across normal shock in DTN.

The presence of an active pool of free radicals marks the active reaction zones in the flow field. Contours of all free radicals and products are shown in Fig. 14. The shear layer anchored to the exit of the inner nozzle sustains a higher concentration of them. The presence of these free radicals is strongly influenced by the temperature and pressure of the compressible flow field. Hence this simulation could depict the reaction profile of the free shear layer and the flow field associated with the complex shock system. The dynamics of the shock structure has a significant influence on the reacting free shear layer coexisting with it. Shock structure depends on the positioning of the nozzle, thrust chamber operating conditions, and the ambient conditions. Chemical radical profile predicted in the present study a vital input for the propulsion designer to fine-tune the optimum performance in off-design operating conditions during the ascend of a spacecraft.

6. CONCLUSIONS

Numerical simulations of the turbulent compressible reacting flows in a novel dual throat thruster have been carried out using a well-validated HLLC scheme based finite volume solver with a multi-step finite rate chemistry model for hydrocarbon/hydrogen-oxygen mixed-mode combustion. The following are the major observations and conclusions based on the results of the present study.

Dual throat nozzles exhibit an interesting flow characteristic when tested for a typical off-design operating condition as considered in the present work. Mach reflection shock interaction pattern results at the exit of the inner nozzle due to the adverse pressure conditions persisting at the secondary throat region. The shear layer emanating from the exit of the inner nozzle is found to anchor stably and thickens smoothly as it progresses downstream. The present study could portray the species profile of the free shear layer in a flow field associated with the complex shock system.

Reacting flow simulation of the present dual throat nozzles could demark the reactive shear layer in a typical tri-propellant engine thrust chambers powered independently by RP1-O₂ and H₂-O₂ combustion. Variations in the concentrations of the free-radicals and the products are accurately captured in active combustion zones with the presence of Mach reflection shock interaction and a high-speed shear layer of sharp gradients.

REFERENCES

- Cheng, T., J. Wehrmeyer, R. Pitz, J. R. O. Jarret and G. Northam (1991). Finite-rate chemistry effects in a Mach 2 reacting flow, in '27th Joint Propulsion Conference. 2320.
- Deepu, M., M. P. Dhrishit and S. Shyji (2017). Numerical simulation of high speed reacting shear layers using AUSM+-up scheme-based unstructured finite volume method solver. *International Journal of Modeling, Simulation, and Scientific Computing* 8(03), 1750020.
- Deepu, M., S. S. Gokhale and S. Jayaraj (2007). Numerical modelling of scramjet combustor. *Defence Science Journal* 57(4), 367.
- Deere, K. (2003). Summary of fluidic thrust vectoring research at NASA Langley Research Center. In *21st AIAA applied aerodynamics conference* (p. 3800).
- Dharavath, M., P. Manna and D. Chakraborty (2017). Numerical simulation of hydrogen air supersonic coaxial jet. *Journal of The Institution of Engineers (India): Series C* 98(5), 575–585.
- Drummond, J. P., R. C. Rogers and M. Y. Hussaini (1987). A numerical model for supersonic reacting mixing layers. *Computer Methods in Applied Mechanics and Engineering* 64(1-3), 39–60.
- Ewen, R. and C. J. O'Brien (1986). Dual throat thruster test results. In *22nd Joint Propulsion Conference*, p. 1518.

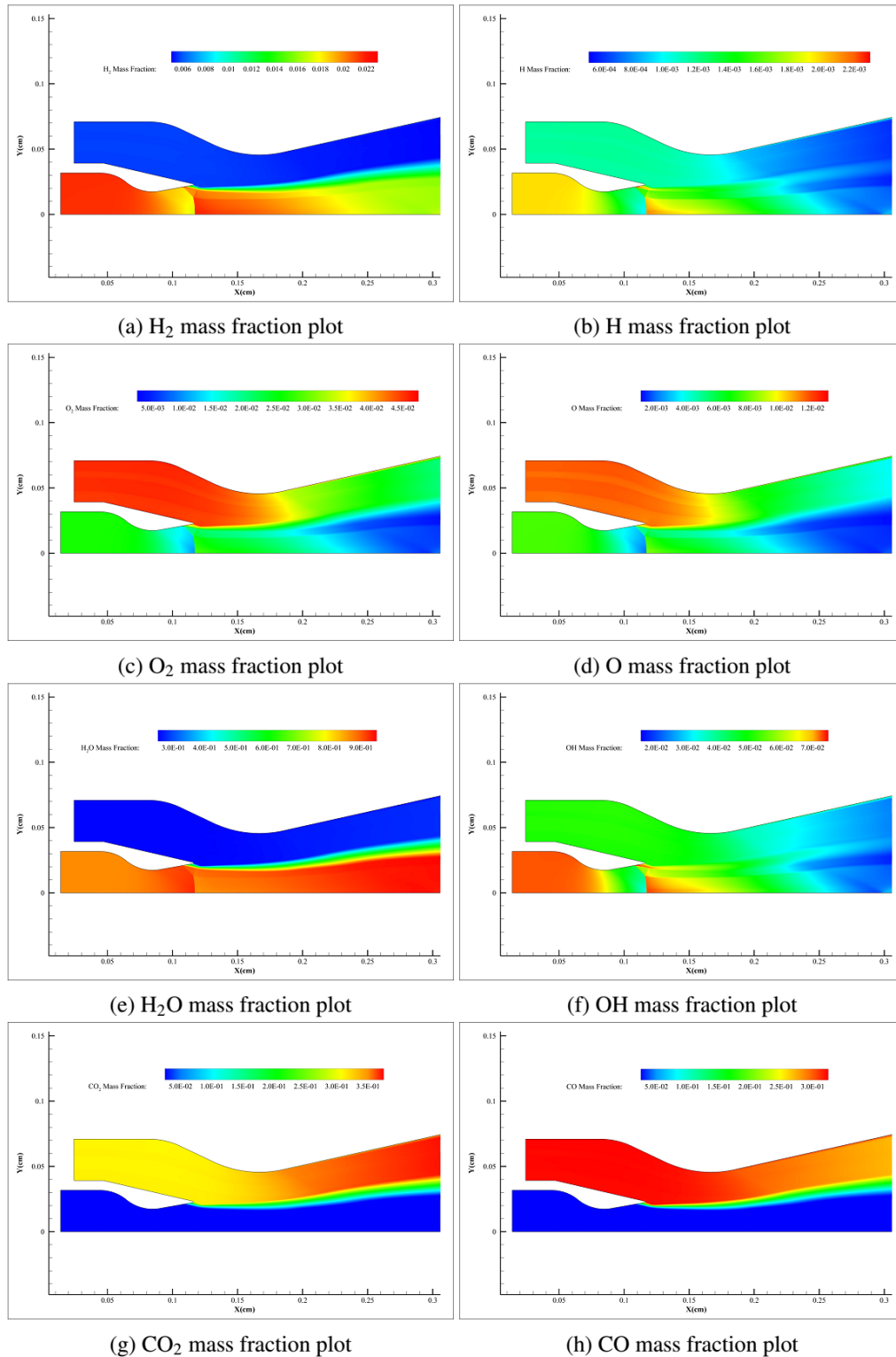


Fig. 14. Contours of species mass fraction.

Goracke, B., D. Levack and G. Johnson (1995). Tripropellant engine option comparison for ssto. in *Space Programs and Technologies Conference*, p. 3609.

Hagemann, G., H. Immich, T. Nguyen and G.

Dumnov (2004). Rocket engine nozzle concepts. *Liquid Rocket Thrust Chambers: Aspects of Modeling, Analysis, and Design. Progress in Astronautics and Aeronautics*, 200.

- Hagemann, G., H. Immich, T. V. Nguyen and G. E. Dumnov (1998). Advanced rocket nozzles. *Journal of Propulsion and Power* 14(5), 620–634.
- Lundgreen, R. B., G. R. Nickerson and C. J. Obrien (1978). Dual throat thruster cold flow analysis. *NASA Report No 32666F*.
- Martin, J. A., T. Vongpaseuth and G. Venkatasubramanyam (1996). Russian rd-704 for single-stage vehicles. *Journal of spacecraft and rockets* 33(2), 309–311.
- Meagher, G. M. (1981). Dual nozzle aerodynamic and cooling analysis study. *NASA Report No NASA-CR-161677*.
- Menter, F. R. (1994). Two-equation eddy-viscosity turbulence models for engineering applications. *AIAA journal* 32(8), 1598–1605.
- Nguyen, T., J. Hyde and M. Ostrander (1988). Aerodynamic performance analysis of dual-fuel/dual-expander nozzles. In *24th Joint Propulsion Conference* (p. 2818).
- Obrien, C. J. (1982). Dual nozzle design update. In *18th Joint Propulsion Conference* (p. 1154).
- Palaniswamy, S., U. Goldberg, O. Perroomian and S. Chakravarthy (2001). Predictions of axial and transverse injection into supersonic flow. *Flow, turbulence and combustion* 66(1), 37–55.
- Shyji, S., M. Deepu, N. A. Kumar and T. Jayachandran (2017). Numerical Studies on Thrust Augmentation in High Area Ratio Rocket Nozzles by Secondary Injection. *Journal of Applied Fluid Mechanics* 10(6).
- Toro, E. F. (2009). The HLL and HLLC Riemann solvers, in ‘Riemann Solvers and Numerical Methods for Fluid Dynamics. Springer, pp. 315–344.
- Toro, E. F., M. Spruce, and W. Speares (1994). Restoration of the contact surface in the HLL-Riemann solver. *Shock Waves* 4, 25–34.
- Vongpaseuth, T., G. Venkatasubramanyam, and J. Martin (1995). Russian tri-propellant engines for SSTO. In *31st Joint Propulsion Conference and Exhibit* (p. 2952).
- Wang, T. S. (2001). Thermophysics characterization of kerosene combustion. *Journal of Thermophysics and Heat Transfer* 15(2), 140-147.
- Wang, Y., J. Xu and S. Huang (2017). Study of starting problem of axisymmetric divergent dual throat nozzle. *Journal of Engineering for Gas Turbines and Power* 139(6), 062602.